WATER RESOURCES RESEARCH, VOL. 40, W10101, doi:10.1029/2003WR002948, 2004

Three-phase flow analysis of dense nonaqueous phase liquid infiltration in horizontally layered porous media

E. L. Wipfler
Netherlands Institute of Applied Geoscience, TNO-NITG, Utrecht, Netherlands

M. I. J. van Dijke
Institute of Petroleum Engineering, Heriot-Watt University, Riccarton Campus, Edinburgh, UK

S. E. A. T. M. van der Zee
Department of Environmental Sciences, Wageningen University, Wageningen, Netherlands

Received 28 November 2003; revised 12 May 2004; accepted 4 June 2004; published 1 October 2004.

[1] We considered dense nonaqueous phase liquid (DNAPL) infiltration into a water-unsaturated porous medium that consists of two horizontal layers, of which the top layer has a lower intrinsic permeability than the bottom layer. DNAPL is the intermediate-wetting fluid with respect to the wetting water and the nonwetting air. The layer interface forms a barrier to DNAPL flow, which causes the DNAPL to spread out horizontally just above the interface. An analytical approximation has been developed to estimate the DNAPL pressure and saturation and the horizontal extension of the DNAPL above the layer interface at steady state for low water saturations. The analytical approximation shows that the DNAPL infiltration is determined by five dimensionless numbers: the heterogeneity factor γ, the capillary pressure parameter λ, the gravity number N_g, the ratio of the capillary and gravity numbers N_c/N_g, and the critical DNAPL pressure P_o^c. Its predictions were compared with the results of a numerical three-phase flow simulator for a number of parameter combinations. For most of these combinations the analytical approximation predicts the DNAPL pressure and saturation profiles at the interface adequately. Using the analytical approximation, we carried out a sensitivity study with respect to the maximum horizontal extension of the plume. The extension of the plumes appears to be highly sensitive to variation of the dimensionless numbers P_o^c, λ and γ. *INDEX TERMS:* 1831 Hydrology: Groundwater quality; 1875 Hydrology: Unsaturated zone; 3210 Mathematical Geophysics: Modeling; 3230 Mathematical Geophysics: Numerical solutions; *KEYWORDS:* heterogeneous porous media, three-phase flow, unsaturated zone

Citation: Wipfler, E. L., M. I. J. van Dijke, and S. E. A. T. M. van der Zee (2004), Three-phase flow analysis of dense nonaqueous phase liquid infiltration in horizontally layered porous media, *Water Resour. Res.*, *40*, W10101, doi:10.1029/2003WR002948.

1. Introduction

[2] Infiltration of nonaqueous phase liquid (NAPL) into the subsurface is a serious environmental problem. Although NAPLs may be considered immiscible with water, they usually have water solubilities which exceed water quality standards, and therefore may contribute to groundwater contamination. Several remediation techniques like removal by pumping have been developed to remove NAPL from the subsurface. The effectiveness of these techniques may be poor due to spatial variation of porous medium properties like intrinsic permeability (k) and porosity (ϕ). Understanding the mechanisms that control NAPL behavior in a heterogeneous porous medium and the ability to predict the subsurface distribution of NAPL is important for the success of remediation efforts.

0043-1397/04/2003WR002948$09.00

[3] Capillary forces play an important role in NAPL flow in heterogeneous porous media. In a two-phase system, the capillary pressure, p_c, which is the pressure difference between the wetting and the nonwetting fluid, can be written as [*Leverett*, 1941]:

$$p_c = \gamma_{nw}\sqrt{\frac{\phi}{k}}J(S) \tag{1}$$

where γ_{nw} denotes the interfacial tension between the wetting fluid and the nonwetting fluid. The Leverett J function $J(S)$ depends on the wetting fluid saturation S, but is independent of porous medium and fluid properties. Consequently, if the permeability or the porosity changes between two layers in a porous medium, continuity of capillary pressure forces the fluid saturation to be discontinuous across the interface between these layers. In turn, this may lead to discontinuities in the relative

permeability at the layer interface, as the latter is a function of the fluid saturation. According to Darcy's law

$$u_i = \frac{-kk_{ri}}{\mu_i}\nabla(p_i - \rho_i g z), \quad (2)$$

the Darcy velocity u_i of a given phase i is proportional to the pressure gradient ∇p_i, according to the mobility $(kk_{ri})/\mu_i$, which consists of the intrinsic permeability k, the relative permeability k_{ri} and the viscosity μ_i. In equation (2) ρ_i denotes density of phase i and g denotes the gravitational acceleration, which acts in the direction of the vertical coordinate z. A strong reduction across a (horizontal) interface of the relative permeability of a downward infiltrating fluid may reduce the mobility, which in turn may reduce the fluid velocity across the interface. This often leads to accumulation of the fluid above the interface, as demonstrated by several studies that are outlined below.

[4] The precise effect of changes of porous medium properties at the interface between layers depends on the wetting order of the infiltrating fluid relative to that of the fluids that are present in the medium. When a nonwetting fluid infiltrates (drainage) into a high permeable layer that lies on top of a low permeable layer, fluid will accumulate above the interface between the two layers. Analyses of the effect of low permeable layers on the infiltration of nonwetting fluid have been provided by *van Duijn et al.* [1995], *de Neef and Molenaar* [1997], and *van Dijke and van der Zee* [1998]. *Van Duijn et al.* [1995] mathematically derived a pressure condition in case of discontinuity of permeability or porosity, which admits solutions of the corresponding phase saturations. *De Neef and Molenaar* [1997] studied 2-D infiltration of nonwetting dense nonaqueous phase liquid into a water-saturated porous medium containing a single low permeable lens of finite dimensions with a high entry pressure. They derived an explicit criterion for DNAPL infiltration into the lens. *Van Dijke and van der Zee* [1998] derived expressions for steady state nonwetting air flow below and through a low permeable horizontal layer in an initially water-saturated porous medium (air sparging). They provided an estimate for the radius of influence of the injected air. With a few modifications, their analysis applies also to DNAPL infiltration above a water-saturated low permeable layer. A similar problem has been studied by *Pritchard et al.* [2001] for vertical equilibrium flow over the interface between two layers in layered porous media. Contrary to *de Neef and Molenaar* [1997] and *van Dijke and van der Zee* [1998], *Pritchard et al.* [2001] did not account for capillary pressure.

[5] On the other hand, when a wetting fluid infiltrates (imbibition) in a high permeable layer flow may be enhanced by the high intrinsic permeability, but the wetting fluid relative permeability in such a layer is often strongly reduced. Therefore, when a wetting fluid flows downward from a low permeable layer into a high permeable layer, its mobility usually decreases. Consequently, the wetting fluid has the potential to accumulate above the high permeable layer. This is referred to as the capillary barrier effect. Capillary barriers have been studied extensively with respect to water infiltration into dry sand of which an overview has been provided by *Schroth et al.* [1998].

[6] In this paper, we consider infiltration of an intermediate-wetting fluid in a horizontally layered porous medium as part of a three-fluid phase system. More precisely, in a water wet soil where both water, the wetting fluid, and air, the nonwetting fluid, are present, and DNAPL, the intermediate-wetting fluid, infiltrates. This implies that DNAPL will display wetting fluid behavior with respect to the nonwetting air and nonwetting fluid behavior with respect to the wetting water. The DNAPL infiltrates from a point source into a horizontal low permeable layer, which is located on top of a high permeable layer. The porous medium is unsaturated with water and the water saturation is assumed to be small near the interface between the layers. Because of the low water saturation we expect that near the interface, DNAPL displays mainly wetting fluid behavior, i.e., in interaction with air. Hence the interface between the layers acts as a capillary barrier for the infiltrating DNAPL [*Walser et al.*, 1999; *Wipfler et al.*, 2004]. Note that, if in the given layer configuration the water saturation increases, DNAPL flow through the interface may be enhanced, as DNAPL is nonwetting relative to water.

[7] The objective of this paper is to analyze the DNAPL spreading above the interface using a three-phase flow simulator and by developing an analytical approximation that provides an estimate for DNAPL pressure, saturation and lateral spreading in the area just above the interface when DNAPL flow has reached a steady state. The analytical approximation is compared to numerical calculations with a discussion of differences in the results. The analytical approximation clarifies the above mentioned interaction between capillary forces and heterogeneities in a three-fluid phase system of DNAPL, water and air, a combination of fluids that is often found in environmental problems.

[8] The use of analytical solutions alongside numerical simulations has been fruitful in the above discussed studies by *de Neef and Molenaar* [1997] and by *van Dijke and van der Zee* [1998]. *Van Dijke and van der Zee* [1997] have provided another example of using an approximate analytical solution to investigate a rather complicated three-phase flow problem. They investigated the redistribution (horizontal spreading) of LNAPL on the phreatic surface in a homogeneous porous medium, while incorporating a model for NAPL entrapment in the constitutive relations. However, it should be stressed that the physical problem and the analytical model are entirely different from the work presented in the present paper. The agreement between all of these papers, is that (well defined) simplifications are made to reduce a physical complicated problem to a problem that can be solved analytically.

[9] The present work extends the analytical model of *van Dijke and van der Zee* [1998] where the nonwetting fluid (air) spreads below a low permeable layer in the two-phase system (water and air). The agreement between the papers is that a layered domain is considered and that the same hydraulic functions are used. However, *van Dijke and van der Zee* [1998] considered injection of the nonwetting fluid air, whereas the present paper describes infiltration of the intermediate wetting fluid, i.e., DNAPL in the presence of water and air. Obviously, the direction of the buoyancy forces is different in the two papers, since air flows downward and spreads below the interface. More important, however, is the difference in the way the mobility of the

infiltrating fluids changes at the interface, caused by the difference in wetting order of the fluids, as outlined above.

[10] The analytical approximation identifies the key parameters that define the redistribution of an intermediate wetting fluid in case of horizontally layered porous media in a three-phase system. Furthermore, the analytical approximation can easily be used for parameter combinations where the numerical procedure becomes less stable or requires very long computation times. It may also be helpful to verify newly developed numerical codes.

[11] The paper is organized as follows. In section 2.1 we formulate the (transient) model equations and in section 2.2 we discuss an example simulation to support the analysis of the infiltration problem at steady state. We reformulate the steady state problem in dimensionless form and identify the governing dimensionless numbers in section 3.2. We additionally identify DNAPL flow regimes in section 3.3, which lead to a number of assumptions that will be used in the analytical approximation described in section 3.4. In section 3.4 we derive an ordinary differential equation for the DNAPL pressures at the layer interface that governs the DNAPL flow at steady state, followed by a discussion in section 3.5. In section 4.1 we show the results of numerical calculations and verify the accuracy of the analytical model by the numerical results in section 4.2. In addition, we analytically perform a sensitivity analysis of the effects of the dimensionless numbers on the lateral extension of DNAPL at the interface in section 4.3.

2. Model Equations and Numerical Simulation

2.1. Model Equations

[12] We consider the flow of DNAPL and water in a water wet soil, where additionally air is present at constant pressure ($p_a = 0$). Assuming that both fluids are incompressible and immiscible, the governing equations for the flow of water (w) or DNAPL (o) are the mass balance equation

$$\phi \frac{\partial \overline{S}_i}{\partial t} + \nabla \cdot u_i = 0 \qquad i = w, o. \tag{3}$$

u_i denotes the 3-D Darcy velocity vector of phase i, given by equation (2), where the vertical component z is directed downward, representing the depth below the soil surface. ϕ denotes the effective porosity, $\overline{S}_i$ denotes the effective saturation of phase i and t denotes time. We assume that the soil consists of two horizontal layers, which are isotropic, but which have different soil properties. The effective saturations are related through $\overline{S}_w + \overline{S}_o = \overline{S}_t$ and $\overline{S}_t + \overline{S}_a = 1$, where $\overline{S}_a$ and $\overline{S}_t$ are the effective air and total liquid saturations. Effective saturations have been derived from the actual saturations through

$$\overline{S}_w = \frac{S_w - S_{wr}}{1 - S_{wr}}, \quad \overline{S}_o = \frac{S_o}{1 - S_{wr}}, \quad \overline{S}_t = \frac{S_t - S_{wr}}{1 - S_{wr}}, \tag{4}$$

where S_{wr} is the residual water saturation. In the following we will use the notation S_w, S_o and S_t to denote the effective saturations. We assume that water is the wetting phase, air is the nonwetting phase and DNAPL is the intermediate-wetting phase, i.e., DNAPL is wetting relative to air, but nonwetting relative to water.

[13] The phase pressures p_i are linked through the capillary pressure p_c^{ij} as $p_c^{ij} = p_i - p_j$, $ij = aw, ao, ow$, which in turn are functions of the effective fluid saturations. For the latter, we use scaled variants of the empirical function of *Brooks and Corey* [1966], which account for a distinct entry pressure, p_e, of the nonwetting fluid. For the two-phase air-water system this functional relation takes the form

$$S_w = \left(\frac{p_e}{p_c^{aw}}\right)^{\lambda}, \quad \text{for} \quad p_c^{aw} > p_e, \tag{5}$$

while $S_w = 1$ if $p_c^{aw} \leq p_e$. For the three phase air-DNAPL-water system the relations are

$$S_w = \left(\frac{p_e}{\beta_{ow} p_c^{ow}}\right)^{\lambda} \quad \text{for} \quad \beta_{ow} p_c^{ow} > p_e, \tag{6}$$

while $S_w = 1$ if $\beta_{ow} p_c^{ow} \leq p_e$, and

$$S_t = \left(\frac{p_e}{\beta_{ao} p_c^{ao}}\right)^{\lambda} \quad \text{for} \quad \beta_{ao} p_c^{ao} > p_e, \tag{7}$$

while $S_t = 1$ if $\beta_{ao} p_c^{ao} \leq p_e$. λ and p_e are Brooks and Corey parameters that represent the structure of the porous medium. β_{ow} and β_{ao} are ratios of the involved interfacial tensions, whose values are related as $1/\beta_{ow} + 1/\beta_{ao} = 1$, thus ensuring continuity of S_w between the two-phase and three-phase systems, i.e., when $S_o = 0$ [*Parker and Lenhard*, 1987]. For the functional relation between relative permeability and saturation we use the relationships proposed by *Mualem* [1976],

$$k_{rw} = S_w^{5/2+2/\lambda} \tag{8}$$

and

$$k_{ro} = (S_t - S_w)^{1/2} \left(S_t^{1+1/\lambda} - S_w^{1+1/\lambda}\right)^2. \tag{9}$$

These relationships apply to the three-phase system as well as to the relevant two-phase systems, in the sense that we use $S_t = 1$ in equation (9) for the two-phase water-DNAPL system and that we only use equation (8) for the two-phase air-water system. Hysteresis is not included in the analysis.

[14] Equations (3) and (2) are solved in the axially symmetric domain shown in Figure 1, where r is the radial coordinate. A low permeable horizontal layer lies on top of a high permeable layer, separated by the level $z = z^*$. The level $z = h$ corresponds to the position of the water table. DNAPL is introduced at $z = 0$ for $0 < r < \frac{1}{2}d$ with an infiltration rate of $u = u_{in}$, where d is the diameter of the source area.

[15] Denoting the intrinsic permeability in the high permeable layer as k^+ and in the low permeable layer as k^-, we introduce a contrast in soil properties by setting $k^+ = \gamma^2 k^-$, $\gamma > 1$. γ is the heterogeneity factor. Then, in agreement with the scaling theory of *Leverett* [1941] (see equation (1)), we additionally introduce contrasting entry pressures p_e^+ and p_e^- for the top and bottom layer respectively, with $p_e^+ = p_e^-/\gamma$. At the layer interface two

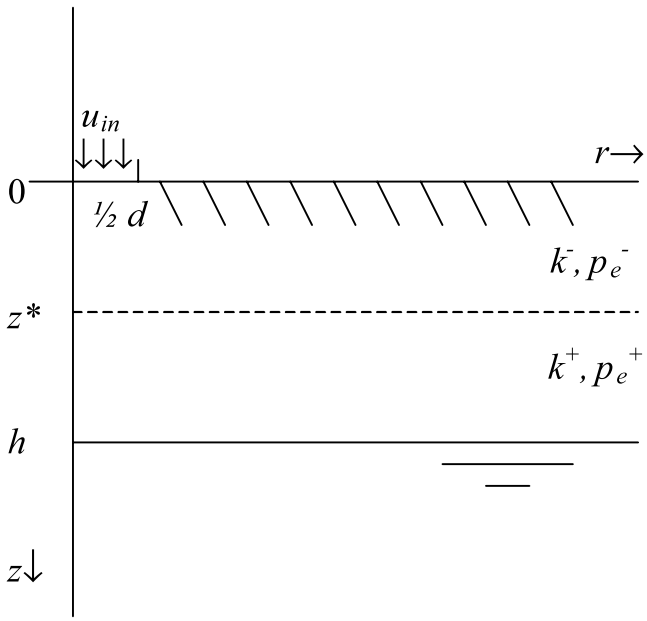

Figure 1. Schematic of the axially symmetric domain with two horizontal layers, separated by the interface at $z = z^*$. DNAPL infiltrates at the soil level $z = 0$ with an infiltration velocity, u_{in}, between $r = 0$ and $r = \frac{1}{2}d$, and the water table is located at $z = h$. The layers have different soil properties; the upper layer is a low permeable layer indicated by k^-, p_e^-, and the lower layer is a high permeable layer indicated by k^+, p_e^+.

conditions apply. Capillary pressure across the interface must be continuous and in addition, conservation of mass implies that the normal component of the flux across the interface must be continuous.

2.2. Example of a Numerical Solution

[16] To get a qualitative picture of the behavior of infiltrating DNAPL in a layered soil, we have carried out an example simulation with parameter values presented in Tables 1 and 2. We will use the results of this calculation to support the subsequent analysis of the infiltration problem. Further details of the simulator and additional calculations are presented in section 4.1. Obviously, the numerical calculation required a finite domain, of which the horizontal extension was taken so large that DNAPL did not reach the right-hand side boundary. At this right-hand side boundary for water the hydrostatic pressure distribution was imposed, with $p_w = 0$ at $z = h$, such that the water saturation near the interface $z = z^*$ was small ($S_w = 0.016$ for this example calculation). For DNAPL a no flow condition was imposed at this boundary. At the left-hand side boundary no-flow conditions were imposed for both water and DNAPL. The bottom boundary was taken well below the level of the water table, where for water the consistent hydrostatic pressure was prescribed, while for DNAPL a pressure smaller than p_w was prescribed, such that DNAPL could move out of the domain through this boundary. The top boundary $z = 0$ was closed to both water and DNAPL, except for the area of the source, where the DNAPL flow rate was imposed as described above.

[17] In Figure 2 we show the numerically obtained DNAPL saturation contours at steady state, i.e., when the amount of DNAPL flowing into and out of the domain are approximately equal and the saturation does not change anymore. The contours show that just above the interface the DNAPL has accumulated and spread out horizontally, indicating that for the present water distribution the high permeable layer indeed acts as a capillary barrier to the DNAPL infiltration. At steady state, water pressures were hydrostatically distributed anywhere in the domain, such that water did not flow anymore. In the entire domain DNAPL saturations were low, i.e., so not exceeding $S_o < 0.032$.

Table 1. Geometry and Porous Medium Properties Used in the Numerical Simulations

Parameter	Value
h, cm	28.4
z^*, cm	8.1
d, cm	1.92
u_{in}, cm s^{-1}	1.667×10^{-8}
ϕ	0.4
k^-, cm^2	6.3821×10^{-8}
p_e^-, Pa	215
λ	2.3
γ	1.9
g, m s^{-2}	9.793

3. Steady State Flow Analysis

3.1. Assumptions

[18] From the example calculation presented in section 2.2 it has become clear that a steady state situation arises, in which the amount of DNAPL flowing into and out of the domain are approximately equal. This steady state allows a number of approximations for the flow equations, such that an analytically treatable problem remains. The eventual analytical flow model, which is discussed in section 3.5 below, deals with the accumulation and horizontal spreading of DNAPL above the interface between the low and the high permeable layers.

[19] The assumptions for the analytical treatment of the steady state DNAPL flow are summarized below. We will specify the conditions for some of these assumptions in section 3.4. (1) Flow of water is negligible, only DNAPL flows. Water pressures are distributed hydrostatically throughout the domain. (2) Distinct flow regimes arise above and below the interface, respectively. Below the interface DNAPL flow is gravity-dominated. Above the interface DNAPL flow occurs at (vertical) gravity-capillary equilibrium. (3) In the neighborhood of the interface the medium is water-unsaturated and water saturations are small. (4) DNAPL saturations are much smaller than 1, although

Table 2. Fluid Properties Used in the Numerical Simulations

Parameter	Value
μ_w, Pa s	1.0×10^{-3}
μ_o, Pa s	2.0×10^{-3}
ρ_w, kg m^{-3}	1000
ρ_o, kg m^{-3}	1600
β_{ao}	1.8
β_{ow}	2.25
β_{aw}	1

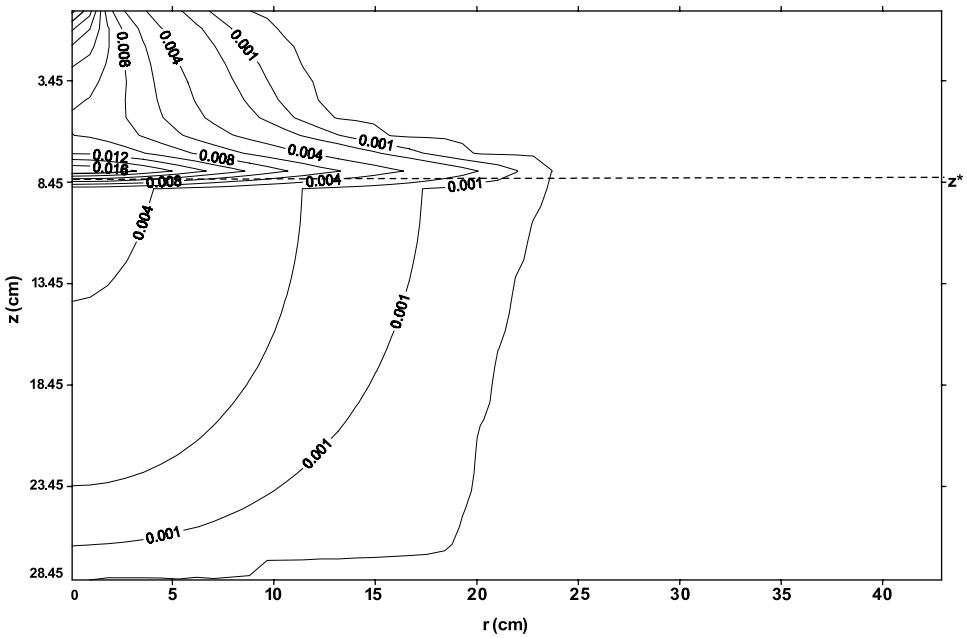

Figure 2. Numerically obtained DNAPL saturation contours at steady state. The horizontal dashed line indicates the interface between the two layers above which the infiltration DNAPL accumulates and spreads. Parameters values used in the calculation can be found in Tables 1 and 2. The water table is located at z = 28.4 m, just below the bottom of the domain.

saturations above the interface are significantly larger than below the interface. For the vertical equilibrium region, sketched in Figure 3, we assume additionally that (5) the height of the vertical equilibrium area is small relative to its width, i.e., the horizontal extension of the DNAPL plume, and (6) infiltration of DNAPL from the top of the domain is replaced by horizontal injection from the axis of (radial) symmetry into the vertical equilibrium region.

3.2. Dimensionless Formulation

[20] To facilitate the analysis of the steady state DNAPL flow, we introduce the dimensionless variables:

$$T = \frac{tU_c}{\phi d},\ R = r/d,\ Z = z/d,\ U_o = u_o/U_c, \tag{10}$$

where $U_c = \frac{k^- \rho_o g}{\mu_o}$ is the intrinsic DNAPL velocity of the low permeable layer. The source diameter, d, is chosen as the characteristic length. Hence we define also the dimensionless distances $H = h/d$ and $Z^* = z^*/d$. Dimensionless pressures are defined as:

$$P_i = \frac{p_i}{p_e^-} \qquad I = w, o. \tag{11}$$

Furthermore, we define the dimensionless constants:

$$N_g = \frac{k^- \rho_o g}{\mu_o u_{in}} \quad \text{and} \quad N_c = \frac{k^- p_e^-}{\mu_o u_{in} d}. \tag{12}$$

N_g is the gravity number and N_c is the capillary number (both related to the low permeable layer). According to assumption 1 the water pressures are distributed as,

$$P_w(Z) = \frac{N_g}{N_c}\frac{\rho_w}{\rho_o}(Z - H). \tag{13}$$

The governing steady state flow equations for DNAPL, following from equations (2) and (3), are

$$\nabla \cdot U_o = 0 \tag{14}$$

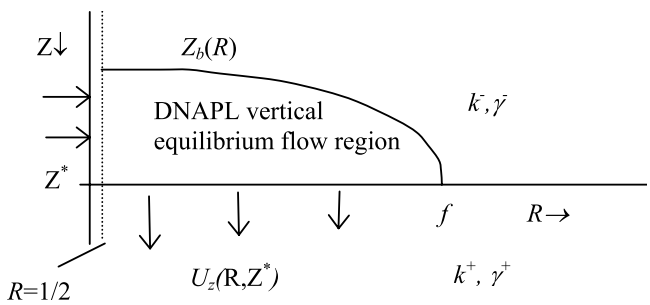

Figure 3. Schematic of the region just above the interface $Z = Z^*$, between the low and high permeable layers, where DNAPL flow is assumed to occur at vertical equilibrium. To derive an analytical approximation for the extent of this region, we assume that rather than from the top, DNAPL enters horizontally via a tube with radius 1/2 located at R = 0 at an (dimensionless) infiltration rate equal to the original rate of $\pi/4N_g$. DNAPL leaves the region through the boundary $Z = Z^*$, where the (vertical) flow velocity is determined by flux continuity to the high permeable lower layer. The region is bounded from above by the (no flow) free boundary at $Z = Z_b(R)$, where the DNAPL saturation is zero. f denotes the maximum horizontal extension of the DNAPL plume at $Z = Z^*$.

with

$$U_o = \begin{cases} k_{ro}\nabla\left(-\frac{N_c}{N_g}P_o + Z\right) & \text{for } Z < Z^* \\ \gamma^2 k_{ro}\nabla\left(-\frac{N_c}{N_g}P_o + Z\right) & \text{for } Z > Z^* \end{cases} \quad (15)$$

for the low and the high permeable layers, respectively. Equations (14) and (15) must be solved for the only remaining unknown P_o, separately on the two subdomains. The solutions are linked by the continuity conditions at the interface for the DNAPL pressure and the vertical component of the DNAPL flux, U_Z, respectively, i.e.,

$$\begin{aligned} \lim_{Z\downarrow Z^*} P_o &= \lim_{Z\uparrow Z^*} P_o \\ \lim_{Z\downarrow Z^*} U_Z &= \lim_{Z\uparrow Z^*} U_Z. \end{aligned} \quad (16)$$

To solve equations (14) and (15), we only need a constitutive relation for the DNAPL relative permeability, k_{ro}. Using the definition for the capillary pressures and the assumption that $P_a = 0$, we rewrite relations (6) and (7) in dimensionless form as

$$S_w = \begin{cases} \hat{S}_w(P_o, P_w) & \text{for } Z < Z^* \\ \hat{S}_w(\gamma P_o, \gamma P_w) & \text{for } Z > Z^* \end{cases} \quad (17)$$

with $\hat{S}_w(P_o, P_w) = (\beta_{ow}(P_o - P_w))^{-\lambda}$ and

$$S_t = \begin{cases} \hat{S}_t(P_o) & \text{for } Z < Z^* \\ \hat{S}_t(\gamma P_o) & \text{for } Z > Z^* \end{cases} \quad (18)$$

with $\hat{S}_t(P_o) = (\beta_{ao}(-P_o))^{-\lambda}$. The difference in the definitions for $Z < Z^*$ and $Z > Z^*$ reflects the contrast in entry pressure between the two layers, i.e., $p_e^+ = p_e^-/\gamma$. Then, the DNAPL relative permeability can be rewritten as

$$k_{ro} = \begin{cases} \hat{k}_{ro}(P_o, P_w) & \text{for } Z < Z^* \\ \hat{k}_{ro}(\gamma P_o, \gamma P_w) & \text{for } Z > Z^* \end{cases} \quad (19)$$

with $\hat{k}_{ro}(P_o, P_w) = k_{ro}(\hat{S}_w(P_o, P_w), \hat{S}_t(P_o))$, while k_{ro} is defined by equation (9).

[21] Notice that the definitions of equations (17)–(19) are valid for $S_w < 1$ and $S_t < 1$, as we will only consider the fluid-unsaturated part of the soil in the subsequent analysis (this is also stated in assumption 3). Consequently, we can also unambiguously define a critical DNAPL pressure P_o^c as a function of P_w, below which the DNAPL saturation is zero. Taking $S_o = S_t - S_w = 0$ in relations (17) and (18), this critical pressure is found as

$$P_o^c = \frac{\beta_{ow} P_w}{\beta_{ow} + \beta_{ao}}. \quad (20)$$

To facilitate the analysis, we have derived in Appendix A an approximate explicit relation between the reduced NAPL relative permeability $\hat{k}_{ro}$ and P_o, P_w. As a result, the relative permeability given by equation (19) is approximated as

$$k_{ro} = \begin{cases} C_k(P_w)\left(P_o - P_o^c\right)^{\frac{5}{2}} & \text{for } Z < Z^* \\ C_k(\gamma P_w)\left[\gamma\left(P_o - P_o^c\right)\right]^{\frac{5}{2}} = & \\ \qquad \gamma^{-\frac{5}{2}\lambda - 2} C_k(P_w)\left(P_o - P_o^c\right)^{\frac{5}{2}} & \text{for } Z > Z^* \end{cases} \quad (21)$$

which applies for small S_o, i.e., when P_o is close to P_o^c, with $C_k(P_w) = \lambda^{5/2}\left(1 + \frac{1}{\lambda}\right)^2 (\beta_{ow} + \beta_{ao})^{5/2} (-P_w)^{-(5/2)\lambda - 9/2}$. Since for the analytical treatment of the flow problem, we assume that the DNAPL saturation is much smaller than 1 (assumption 4), we can use equation (21) in the derivations.

3.3. DNAPL Flow Regimes

[22] To derive an analytical approximation for the lateral extension of the DNAPL at the interface between the high and the low permeable layers, we analyze the regimes of DNAPL flow above and below the interface. The aim of this analysis is to derive the DNAPL pressure distribution within the vertical equilibrium region and the conditions at the various boundaries surrounding this region. A schematic of this vertical equilibrium region is presented in Figure 3, which we explain in detail below. According to assumption 2, the flow in the high permeable layer just below the interface is only vertical and is dominated by gravity. Hence we obtain from equation (15) that

$$U_Z \approx \gamma^2 k_{ro} \quad \text{for } Z > Z^*. \quad (22)$$

Using equation (15), the continuity condition (16) for U_z at the interface yields

$$\lim_{Z\uparrow Z^*} k_{ro}\left(-\frac{N_c}{N_g}\frac{\partial P_o}{\partial Z} + 1\right) \approx \lim_{Z\downarrow Z^*} \gamma^2 k_{ro} \quad (23)$$

According to assumption 4, we may safely assume that the DNAPL saturation is small, hence we use the approximation (21) in relation (23) to obtain

$$\lim_{Z\uparrow Z^*} \frac{\partial P_o}{\partial Z} \approx -\frac{N_g}{N_c}\left(\gamma^{-(5/2)\lambda} - 1\right) \quad (24)$$

for the vertical pressure gradient just above the interface. Since we have $\lambda > 1$, this gradient is approximately equal to N_g/N_c for sufficiently large values of the heterogeneity factor γ. If the gradient is exactly equal to N_g/N_c, DNAPL pressures just above the interface are at vertical equilibrium, as stated in assumption 2. Because of the relatively large absolute value of the power $(5/2)\lambda$, the contrast $\gamma > 1$ needs not be very large to yield a good approximation of the vertical equilibrium condition. Additionally, the pressure derivatives that we obtained from the example calculation of section 2.2 confirm this conclusion. Consequently, we assume that in the region just above the interface, where the DNAPL has spread out horizontally, DNAPL pressures are distributed hydrostatically, i.e.,

$$P_o(R, Z) = P(R) - \frac{N_g}{N_c}(Z^* - Z). \quad (25)$$

where $P(R) = P_o(R, Z^*)$ is the DNAPL pressure at the interface.

[23] On the basis of this pressure distribution, we may explicitly define this vertical equilibrium flow region, which is shown in Figure 3. The region is bounded from above by the level $Z = Z_b(R)$, where the DNAPL saturation is equal to zero, i.e., $P_o(Z_b) = P_o^c$. This is a no-flow boundary for DNAPL. Using equation (25), Z_b is linked to P as

$$Z_b(R) = Z^* + \frac{N_c}{N_g}\left[P_o^c - P(R)\right]. \tag{26}$$

We define the maximum extension of the plume f, which occurs at the interface, i.e., $Z_b(f) = Z^*$. As stated in assumption 6, instead of infiltration from the top, we assume that DNAPL is introduced via a tube with radius 1/2, located at $R = 0$ such that the total dimensionless infiltration rate is equal to the original rate of $\pi/4N_g$. The tube has a height of $Z^* - Z_b(1/2)$. Along $Z = Z^*$ we impose a boundary condition for the vertical velocity component U_Z, which by flux continuity across the interface (equation (16)) follows from equation (22) as

$$U_Z(R, Z^*) = \gamma^2 \lim_{Z \downarrow Z^*} k_{ro}. \tag{27}$$

Obviously, at steady state the total flow rate through the interface equals

$$\int_{1/2}^{f} R U_Z(R, Z^*) dR = \pi/4N_g. \tag{28}$$

Finally, we assume that the height of the vertical equilibrium area is relatively small compared to the horizontal extension of the plume (assumption 5) and that the water saturations are small in this region, as demonstrated in the numerical example of section 2.2. Therefore we may consider P_w and P_o^c, which according to equation (20) depends on the hydraulically distributed P_w, as constant throughout the region. For the water pressure we take the constant value, P_w^*, equal to that at the interface $Z = Z^*$, which follows from equation (13). Consequently, the relative permeability defined by Equation (21) depends on P_o only, i.e., $k_{ro} = \hat{k}_{ro}(P_o, P_w^*)$ in the vertical equilibrium region.

3.4. Analytical Flow Model

[24] Similar to the analysis of *van Dijke and van der Zee* [1998], we solve equation (14) combined with the first expression of equation (15) in the vertical equilibrium region presented in Figure 3, subject to the above described boundary conditions, to obtain the DNAPL pressure at the interface, $P(R) = P_o(R, Z^*)$. Notice that also the free boundary $Z_b(R)$, hence the maximum extension f, is unknown and will be part of the solution. First, we integrate the mass balance equation (14) in radial coordinates over the height of the region, yielding

$$\int_{Z_b}^{Z^*} \left(\frac{\partial R U_R}{\partial R} + R\frac{\partial U_Z}{\partial Z}\right) = 0. \tag{29}$$

Using $U_R(R, Z_b) = U_Z(R, Z_b) = 0$, where U_R and U_Z are the horizontal and vertical components of the DNAPL velocity, respectively, equation (29) becomes

$$\frac{\partial}{\partial R}\left(R\int_{Z_b}^{Z^*} U_R(R, Z) dZ\right) + R U_Z(R, Z^*) = 0. \tag{30}$$

To evaluate the first term of equation (30), we derive from equation (25):

$$\frac{\partial P_o(R, Z)}{\partial R} = \frac{dP(R)}{dR} \quad \text{and } dZ = \frac{N_c}{N_g} dP(R). \tag{31}$$

Using equation (15) and the definition of the reduced relative permeability (21) we find

$$\begin{aligned}\int_{Z_b}^{Z^*} U_R(R, Z) dZ &= -\frac{N_c}{N_g}\int_{Z_b}^{Z^*} \hat{k}_{ro}(P_o(R, Z), P_w^*)\frac{\partial P_o(R, Z)}{\partial R} dZ \\ &= -\frac{N_c^2}{N_g^2} D(P(R))\frac{dP(R)}{dR}\end{aligned} \tag{32}$$

where D is defined as $D(P) = \int_{P_o^c}^{P} \hat{k}_{ro}(\xi, P_w^*) d\xi$.

[25] At the boundary $Z = Z^*$ condition (27) applies, where we use definition (21) to write $\lim_{Z \uparrow Z^*} k_{ro} = \lim_{Z \uparrow Z^*} \hat{k}_{ro}(\gamma P_o, \gamma P_w) = \hat{k}_{ro}(\gamma P, \gamma P_w^*)$. Hence equation (30) is written as

$$\frac{-N_c^2}{N_g^2}\frac{d}{dR}\left\{R D(P)\frac{dP}{dR}\right\} + R\gamma^2 \hat{k}_{ro}(\gamma P, \gamma P_w^*) = 0. \tag{33}$$

Integration of the mass balance equation (30) over R from $R = 1/2$ to $R = f$, to which we apply condition (28), gives the flux boundary condition at $R = 1/2$

$$-2\pi\frac{N_c^2}{N_g^2} R D(P)\left.\frac{dP}{dR}\right|_{R=1/2} = \frac{\pi}{4N_g}. \tag{34}$$

Hence we solve the boundary value problem for P

$$\begin{cases} \dfrac{-N_c^2}{N_g^2}\dfrac{d}{dR}\left\{R D(P)\dfrac{dP}{dR}\right\} + R\gamma^2 \hat{k}_{ro}(\gamma P, \gamma P_w^*) = 0 \quad \text{for } \dfrac{1}{2} < R < f \\ -2\pi\dfrac{N_c^2}{N_g^2} R D(P)\left.\dfrac{dP}{dR}\right|_{R=1/2} = \dfrac{\pi}{4N_g}, \quad P(f) = P_o^c \end{cases} \tag{35}$$

Because the maximum horizontal extension, f, of the DNAPL is unknown, an additional boundary condition is required to solve problem (35). *Van Dijke and van der Zee* [1998] have shown that this condition can be derived considering that at steady state the free boundary $Z_b(R)$ is tangential to the DNAPL flow direction at $R = f$. This leads to the condition for the gradient of P at f

$$\lim_{R \to f}\left(\frac{dP}{dR}(R)\right)^2 = \lim_{R \to f} -\gamma^2 \frac{N_g^2}{N_c^2}\frac{\hat{k}_{ro}(P, P_w^*)}{\hat{k}_{ro}(\gamma P, \gamma P_w^*)}. \tag{36}$$

Table 3. Dimensionless Parameters and Numbers Used in the Computations

Case	γ	λ	P_o^c	$\frac{N_c}{N_g}$	$\frac{1}{N_g}$, $\times 10^{-6}$
1	1.9	2.3	−5.126	0.716	3.334
2	1.9	2.3	−3.611	0.716	3.334
3	1.9	2.3	−5.265	0.716	3.334
4	1.9	2.3	−5.126	0.573	3.334
5	1.9	2.3	−5.126	0.955	3.334
6	1.7	2.3	−5.126	0.716	3.334
7	2.05	2.3	−5.126	0.716	3.334
8	1.9	2.0	−5.126	0.716	3.334
9	1.9	2.5	−5.126	0.716	3.334
10	1.9	2.3	−5.126	0.716	2.500
11	1.9	2.3	−5.126	0.716	4.168
12	1.9	2.3	−5.126	0.716	3.334

Since for $R \rightarrow f$ P approaches P_o^c, we apply the approximations equation (21) to obtain the boundary condition

$$\frac{dP}{dR}(f) = -\gamma^{-\frac{5}{4}\lambda}\frac{N_g}{N_c}. \tag{37}$$

[26] We iteratively solve the differential equation of problem (35) as an initial value problem starting at $R = f$, while varying the values of f, until the condition at $R = 1/2$ is matched. Further detail of the numerical solution of problem (35) is given by *van Dijke and van der Zee* [1998]. After the solution for P and f is obtained, the full solution for the DNAPL pressure P_o in the vertical equilibrium region can immediately be derived from equation (25).

3.5. Discussion

[27] Mathematically, problem (35) is the same as the flow problem studied by *van Dijke and van der Zee* [1998]. However, as mentioned in the introduction, the underlying physical problem exhibits two important differences. On the one hand, we consider a three-phase system instead of a two-phase system, in which P_o^c reflects the effect of the presence of the (wetting) water phase on the flow of the (intermediate wetting) DNAPL phase. In the limiting case, water is entirely absent, i.e., when $P_w \rightarrow -\infty$ and, according to equation (20), $P_o^c \rightarrow -\infty$, DNAPL will spread infinitely at the interface. Hence we may expect the DNAPL spreading to grow with decreasing P_o^c.

[28] On the other hand, whereas in the model of *van Dijke and van der Zee* [1998] the heterogeneity reduces both the intrinsic permeability and the relative permeability to cause the infiltrating fluid to spread near the interface between the layers, the heterogeneity has opposite effects on these parameters in the present problem. Going from the low to the high permeable layer, the effect of the heterogeneity can easily be illustrated by considering the approximation for the DNAPL relative permeability, equation (21). Between the low permeable layer and the high permeable layer the intrinsic permeability increases with a factor γ^2 whereas the relative permeability reduces, according to the approximation, with a factor $\gamma^{-(5/2)\lambda-2}$. Considering the approximate vertical flux through the interface given by equation (27), we still find an overall reduction of the mobility of $\gamma^{-(5/2)\lambda}$.This mobility reduction illustrates that increasing either γ or λ, both of which are always larger than 1, enhances the spreading of the DNAPL.

[29] Additional to the discussed dimensionless numbers P_o^c, γ and λ, problem (35) also contains the dimensionless numbers N_g and N_c representing the ratio between gravity, viscous forces and capillary forces, although these numbers appear in the combinations N_c/N_g and $1/N_g$. Using the analytical approximation, we will show the effect of each of these numbers on the DNAPL spreading in the next section.

4. Results and Discussion

4.1. Numerical Computations

[30] We have carried out a number of flow calculations for the full problem of DNAPL infiltration described in section 2.1 and compare the resulting steady state DNAPL distributions with those computed from the analytical approximation of section 3. The simulations have been carried out using a fully implicit, 2-D axially symmetric, integrated finite difference multiphase flow code called STOMP with fully implicit time differencing [*White and Oostrom*, 1996]. In this code, the set of equations (3) and (2) are solved with a multivariable, residual based Newton-Raphson iteration technique. Upwind interfacial averaging is used to approximate the relative permeabilities. Further details of the simulator are given by *White and Oostrom* [1996].

[31] The boundary conditions for the simulations have been imposed as described in section 2. The 2-D computational domain consisted of 6210 cells. The grid was refined near the source and the layer interface, with the horizontal and vertical grid spacing varying from $\Delta r = 0.12$ cm to $\Delta r = 0.6$ cm and from $\Delta z = 0.04$ cm to $\Delta z = 0.8$ cm, respectively. The values of the nontransformed physical soil and fluid parameters, which were used in the simulator, are presented in Tables 1 and 2. These have been taken for the base case (case 1), of which preliminary results have been presented in section 2.

[32] Compared to this base case, the dimensionless numbers defined in section 3, have been varied as indicated in Table 3. In cases 2 and 3 P_o^c has been varied by adjusting the hydrostatic water pressure, i.e., by varying h. In cases 4 and 5 the ratio N_c/N_g has been varied by varying the source diameter d, in cases 6 and 7 the capillary contrast γ has been varied, in cases 8 and 9 the porous medium property λ has been varied and in cases 10 and 11 N_g has been varied by varying the infiltration velocity u_{in}. In case 12 the DNAPL has been replaced by an LNAPL. For this case the NAPL density has been given the value ρ_o = 800 kg m^{-3}. By simultaneously increasing the values of k^- to 1.2764 10^{-7} cm^2 and of d to 3.84 cm, the dimensionless numbers have been kept the same as for case 1.

[33] For the base case, we found that the spreading of the plume above the interface is sensitive to the vertical discretization. For example, decreasing the Δz from the cells around the interface from 0.08 cm to 0.04 cm increased the spreading of the plume by up to 2.5%. Because of computational restrictions we have not decreased the grid size any further. This may imply that the simulator slightly underpredicts the spreading of the plume. In every case the flow became stationary. We defined the steady state time as the time beyond which the flux across the interface is more than 99.4% of the infiltrating flux. The steady state time for the cases 1 to 12 varied between 28.4 yr. (case 8) and 80 yr.

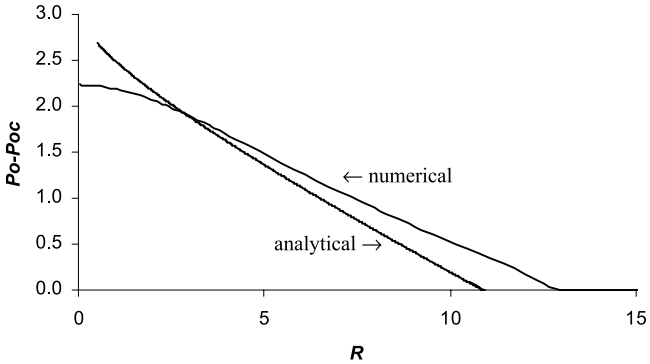

Figure 4. Dimensionless numerically and analytically calculated DNAPL pressure profiles at the interface between the low and the high permeable layers for the parameters of case 1. When $P_o - P_o^c = 0$, the maximum extension of the plume is reached.

(case 9). The computation time was approximately 4 hours using a 300 MHz processor.

[34] Note that the scale of the simulated flow problems is smaller than for most realistic problems, because of restrictions concerning convergence, grid size and computation time. However, the dimensionless analysis shows how the simulations can be scaled up without changing the results. E.g., multiplication of the extension of the domain, the diameter of the source, d, the intrinsic permeability of the low permeable layer, k^-, and the entry pressure, p_e^-, by the same factor, keeps the dimensionless numbers the same as in the presented calculations. Furthermore, a larger and probably more realistic extension of the plume above the layer interface can be obtained by increasing γ or λ, as discussed in section 3.5. However, increasing these factors leads to numerical convergence problems and it requires a much finer grid and significantly larger computation times. Fortunately, the analytical approximation still provides a good estimate of the plume extension at steady state as we will show in the next subsection.

4.2. Comparison of Analytical and Numerical Results

[35] In Figure 4 both the analytical and the numerical solutions for the DNAPL pressure $P_o - P_o^c$ at the interface level $Z = Z^*$ are presented as a function of the radial coordinate R for the parameters of case 1. The maximum horizontal extension of the plume f is attained where $P_o - P_o^c = 0$. The profiles show good agreement, although near $R = 1/2$ the two solutions deviate slightly, which is probably caused by the different DNAPL inflow conditions. Furthermore, the analytical solution underestimates the extension of the plume by about 15%. The assumptions in the analytical approximation of strictly gravity-driven flow below the layer interface and of complete vertical pressure equilibrium just above the interface contribute both to this underestimation. In addition, in the analytical approximation P_o^c has been assumed constant, equal to the value at $Z = Z^*$, throughout the vertical equilibrium region, which is a slight overestimation of the numerically obtained values.

[36] For comparison, we present in Figure 5 the analytically and numerically calculated DNAPL saturation profiles at the interface for the parameters of case 1. For the analytical approximation, this profile has been calculated from the $P_o - P_o^c$ values presented in Figure 4, using equations (17) and (18), where for the water pressure the value $P_w(Z^*)$ has been taken from the hydrostatic distribution (13). The agreement between the two solutions is similar to that for the pressure profiles of Figure 4, although the agreement is worse near $R = 1/2$ as a result of the nonlinear relation between saturation and pressure.

[37] To quantify the agreement between the analytically and numerically obtained solutions, we have compared the maximum extensions of the plume at $Z = Z^*$, which we refer to as f_a and f_n, respectively, through the relative error $(f_n - f_a)/f_n$. In Figure 6 the relative error is presented as a function of the normalized dimensionless parameters. As shown in Figures 4 and 5, for case 1 $f_a = 10.8$ and $f_n = 12.7$, such that the relative error of the reference case was 14.9%. According to Figure 6, increasing either λ or γ results in a better agreement of the analytical approximation with the numerical calculation, whereas $1/N_g$ and N_g/N_c hardly affect the accuracy of the analytical solution. As discussed in section 3.5 both γ and λ lead to an increase of the mobility difference across the interface which increases the agreement with the assumptions underlying the analytical approximation. Furthermore, if the critical DNAPL pressure P_o^c decreases, the relative error decreases. Notice that a decrease of P_o^c corresponds to an increase of the normalized value, as P_o^c is a negative value. Finally, the analytical approximation for the LNAPL simulation is equally accurate as for DNAPL. For this case the numerically obtained extension $f_n = 12.9$, with a relative error of 16.3%.

4.3. Sensitivity Analysis

[38] To quantify the effect of the dimensionless parameters on the spreading of the plume above the interface, we have performed a sensitivity analysis for the horizontal extension f of the plume using the analytical approximation. The analytically calculated extensions f_a of the plume are shown in Figure 7, normalized by the value $f_{a1} = 12.7$ for case 1, as $(f_a - f_{a1})/f_{a1}$. Notice that we have considered extensions for a fairly wide range of the parameters, which we would not have been able to obtain numerically because of the computational problems discussed above, although convergence restrictions of the analytical approximation

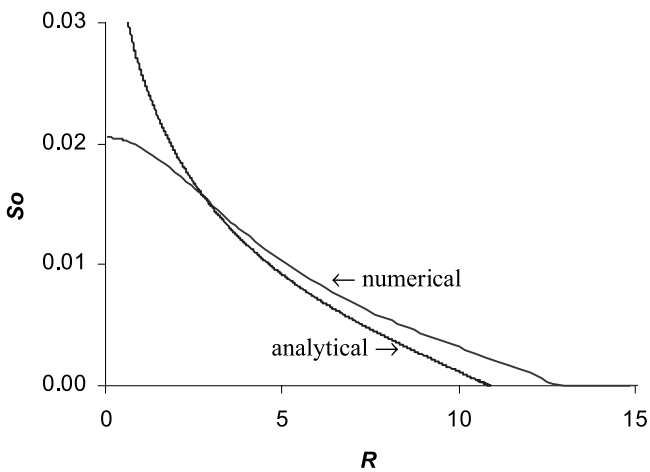

Figure 5. Numerically and analytically calculated DNAPL saturations at the interface between the low and the high permeable layers for the parameters of case 1.

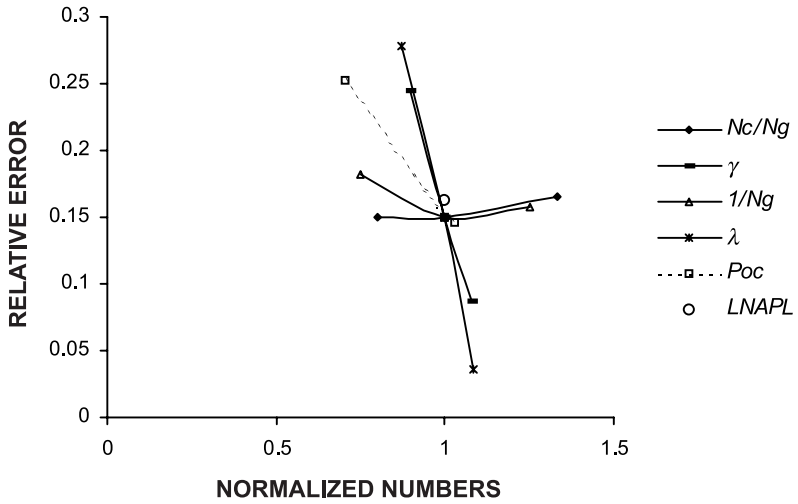

Figure 6. Relative error of the numerically and analytically obtained plume extension as a function of the dimensionless parameters. The dimensionless parameters are normalized by those of case 1. The LNAPL simulation has been carried out for the parameters of case 1 but with a different NAPL density.

still require a limited increase of the normalized P_o^c and λ. The extension of the plume appears to be particularly sensitive to λ and γ, because these parameters strongly affect the mobility differences across the interface. The cases with larger λ and γ values are more interesting than those with smaller values, as the former give very good approximations of the numerically obtained plume extension, according to Figure 6, and are difficult to obtain numerically. In agreement with the discussion of section 3.5 the value of P_o^c has a considerable effect on the plume extension. When P_o^c decreases (i.e., when the normalized P_o^c increases) less water is present and the NAPL can spread out further. Similarly, increasing the value of N_c/N_g, which represents the absolute value of the entry pressures, as $N_c/N_g = p_e^-/(\rho_o g)$, leads to a larger extension. However, from Figure 6 we conclude that the corresponding analytical approximations to the numerical results are not increasingly more accurate. Finally, $1/N_g$, which represents the effect of the infiltration rate, has only a small effect on the spreading of the plume.

5. Conclusions

[39] We have considered DNAPL infiltration into a water-unsaturated porous medium that consists of two horizontal layers, of which the top layer has a lower intrinsic permeability than the bottom layer. DNAPL is intermediate-wetting relative to the wetting water and the nonwetting air. We have demonstrated that the layer interface forms a barrier to DNAPL flow due to the fact that the DNAPL mobility is lower in the high permeable layer, which causes the DNAPL to spread out horizontally just above the

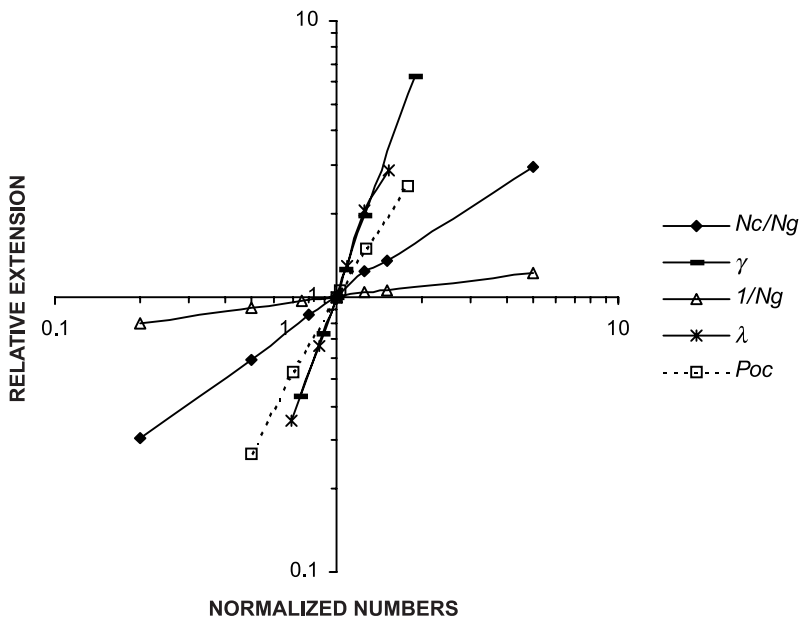

Figure 7. Sensitivity of the extension of the plume at the interface, *f*, to dimensionless parameters relative to the extension for case 1. Also, the dimensionless numbers are normalized by those of case 1.

interface. As a result, the DNAPL pressure distribution just above the layer interface is close to vertical equilibrium, while below the interface DNAPL flow is approximately gravity driven. On the basis of these observations, we have developed an analytical approximation to estimate the DNAPL pressure and saturation and the horizontal extension of the DNAPL plume just above the layer interface at steady state for low water saturations.

[40] The analytical approximation shows that the steady state DNAPL infiltration is determined by 5 dimensionless numbers: the heterogeneity factor γ, the Brooks and Corey capillary pressure parameter λ, the gravity number N_g, the ratio of the capillary and gravity numbers N_c/N_g, and the critical DNAPL pressure P_o^c, which indicates the effect of the water saturation on the flow of DNAPL.

[41] To test the validity of the analytical approximation, we have compared its predictions with the results of a three-phase flow simulator for a number of parameter combinations. For most of these combinations the analytical approximation predicts the DNAPL pressure and saturation profiles at the interface adequately, although it slightly underestimates the horizontal spreading of the plume at the interface. We have shown that for increasing γ and λ, which lead to larger mobility differences across the layer interface, the accuracy of the approximation improves. The approximation improves also for decreasing P_o^c, indicating lower water saturations. In general the analytical approximation improves when the horizontal spreading is larger. The analytical model provides an accurate prediction of the numerically obtained horizontal spreading when the DNAPL is replaced by an LNAPL under otherwise similar conditions.

[42] Using the analytical approximation, we have carried out a sensitivity study with respect to the maximum horizontal extension of the plume. It turns out that the extension of the plumes appears to be highly sensitive to variation of the dimensionless numbers P_o^c, λ and γ. The extension increases for increasing values of λ and γ and for decreasing values of P_o^c.

Appendix A: Relative Permeability Approximation

[43] For P_o close to the critical NAPL pressure, P_o^c, the reduced NAPL relative permeability $\hat{k}_{ro}$ can be approximated by an expansion in terms of $P_o - P_o^c$. From equation (18) follows that

$$\hat{S}_t(P_o) = \left(\frac{-1}{\beta_{ao}P_o}\right)^{\lambda} = \left(\frac{\frac{-1}{\beta_{ao}P_o^c}}{\frac{P_o-P_o^c}{P_o^c}+1}\right)^{\lambda} = (-P_w)^{-\lambda}\left(1-\beta_{ao}\frac{P_o-P_o^c}{-P_w}\right)^{-\lambda}, \quad \text{(A1)}$$

where we have used definition (20) for P_o^c and the constraint $1/\beta_{ao} + 1/\beta_{ow} = 1$ to find $P_o^c = P_w/\beta_{ao}$. Using the binomial expansion $(1+x)^{\alpha} = 1 + \alpha x + O(x^2)$ for small x, we obtain for $\hat{S}_t$ the first-order approximation

$$\hat{S}_t(P_o) \approx (-P_w)^{-\lambda}\left(1+\lambda\beta_{ao}\frac{P_o-P_o^c}{-P_w}\right). \quad \text{(A2)}$$

Similarly, we approximate $\hat{S}_w$, defined in equation (17), by

$$\hat{S}_w(P_o,P_w) = (-P_w)^{\lambda}\left(1-\beta_{ow}\frac{P_o-P_o^c}{-P_w}\right)^{-\lambda} \approx (-P_w)^{-\lambda}\left(1+\lambda\beta_{ow}\frac{P_o-P_o^c}{-P_w}\right) \quad \text{(A3)}$$

where we have again used definition (20) for P_o^c to find $P_o^c - P_w = (-P_w)/\beta_{ow}$. Note that by introducing P_o^c into equation (A1) we have obtained an artificial dependence of S_t on P_w. We did this to obtain a similar form of the equation as equation (A3).

[44] To approximate the NAPL relative permeability, we substitute expressions (A1) and (A3) in equation (9) to find

$$\hat{k}_{ro}(P_o,P_w) \approx \lambda^{1/2}(\beta_{ao}+\beta_{ow})^{1/2}(P_w)^{-(5/2)\lambda-5/2}\left(P_o-P_o^c\right)^{1/2} \cdot\left[\left(1+\lambda\beta_{ao}\frac{P_o-P_o^c}{-P_w}\right)^{1+1/\lambda} -\left(1+\lambda\beta_{ow}\frac{P_o-P_o^c}{-P_w}\right)^{1+1/\lambda}\right]^2 \quad \text{(A4)}$$

Using again the binomial expansion, we obtain the final approximation

$$\hat{k}_{ro}(P_o,P_w) \approx C_k(P_w)\left(P_o-P_o^c\right)^{5/2} \quad \text{(A5)}$$

where $C_k(P_w) = \lambda^{5/2}\,(1+\frac{1}{\lambda})^2(\beta_{ow}+\beta_{ao})^{5/2}\,(-P_w)^{-(5/2)\lambda-9/2}$.

Notation

C_k	DNAPL relative permeability coefficient.
d	diameter of DNAPL source, m.
D	dimensionless relative permeability integral.
f	dimensionless radial position of the free boundary Z_b of the DNAPL plume at $Z = Z^*$.
g	gravity, m s^{-2}.
$h(H)$	(dimensionless) distance from the soil surface to the water table, m.
k	intrinsic permeability, m^2.
k_{ri}	relative permeability of phase i.
$\hat{k}_{ri}$	reduced relative permeability of phase i.
N_c	capillary number.
N_g	gravity number.
P	dimensionless DNAPL pressure at $Z = Z^*$.
$p_i(P_i)$	(dimensionless) pressure phase i, Pa.
$p_c^{ij}(P_c^{ij})$	(dimensionless) capillary pressure fluid i and j, Pa.
p_e	entry pressure, Pa.
P_o^c	dimensionless critical NAPL pressure, Pa.
$r(R)$	(dimensionless) radial coordinate, m.
$S_i(\bar{S}_i)$	(effective) saturation phase i.
$t(T)$	(dimensionless) time, s.
$u_i(U_i)$	(dimensionless) velocity of fluid phase i, m s^{-1}.
u_{in}	infiltration velocity, m s^{-1}.
U_c	characteristic velocity, m s^{-1}.
$z(Z)$	(dimensionless) vertical coordinate, m.
β_{ij}	scaling coefficients for fluid phase i and j.
γ	heterogeneity factor.
γ_{nw}	interfacial tension between the wetting and the nonwetting fluid, N m^{-1}.

λ Brooks and Corey porous medium parameter.
μ_i viscosity phase i, Pa s.
ρ_i density phase i, kg m^{-3}.
ϕ effective porosity.

Subscripts
a air.
b boundary.
o DNAPL.
r residual.
R radial direction.
t total.
w water.
Z vertical direction.

Superscripts
c critical.
$+$ high permeable porous medium.
$-$ low permeable porous medium.
$*$ layer interface.

[45] **Acknowledgments.** This research was conducted as part of the research project ISBN-REM funded by the Environment and Climate Program of the European Commission (DG-XII D-1) contract ENV4-CT97-0612. We thank M. Oostrom from the Pacific Northwest National Laboratory for providing the numerical code STOMP for the multiphase flow calculations.

References

Brooks, R. H., and A. T. Corey (1966), Properties of porous media affecting fluid flow. J, *Irrig. Drain. Div. Am. Soc. Civ. Eng.*, *92*, 61–88.

de Neef, M. J., and J. Molenaar (1997), Analysis of DNAPL infiltration in a medium with a low permeability lens, *Comput. Geosci.*, *1*(2), 191–214.

Leverett, M. C. (1941), Capillary behavior in porous solids, *Trans. Am. Inst. Min. Metall. Pet. Eng.*, *142*, 152–169.

Mualem, Y. (1976), A new model for predicting the hydraulic conductivity of unsaturated porous media, *Water Resour. Res.*, *12*(3), 513–522.

Parker, J. C., and R. J. Lenhard (1987), A model for hysteretic constitutive relations governing multiphase flow: 1. Saturation-pressure relations, *Water Resour. Res.*, *23*(12), 2187–2196.

Pritchard, D., A. W. Woods, and A. J. Hogg (2001), On the slow draining of a gravity current moving through a layered permeable medium, *J. Fluid Mech.*, *444*, 23–47.

Schroth, M. H., J. D. Istok, and J. S. Selker (1998), Three-phase immiscible fluid movement in the vicinity of textural interfaces, *J. Contam. Hydrol.*, *32*, 1–23.

van Dijke, M. I. J., and S. E. A. T. M. van der Zee (1997), A similarity solution for oil lens redistribution including capillary forces and oil entrapment, *Transp. Porous Media*, *29*, 99–125.

van Dijke, M. I. J., and S. E. A. T. M. van der Zee (1998), Modeling of air sparging in a layered soil: Numerical and analytical approximations, *Water Resour. Res.*, *34*(3), 341–353.

van Duijn, C. J., J. Molenaar, and M. J. de Neef (1995), Effects of capillary forces on immiscible two-phase flow in heterogeneous porous media, *Transp. Porous Media*, *21*, 71–93.

Walser, G. S., T. H. Illangasekare, and A. T. Corey (1999), Retention of liquid contaminants in layered soils, *J. Contam. Hydrol.*, *39*, 91–108.

White, M. D., and M. Oostrom (1996), STOMP, Subsurface Transport Over Multiple Phases, theory guide, *Rep. PNNL-11217*, Pac. Northwest Natl. Lab., Richland, Wash.

Wipfler, E. L., M. Ness, G. D. Breedveld, A. Marsman, and S. E. A. T. M. van der Zee (2004), Infiltration and redistribution of LNAPL into unsaturated layered porous media, *J. Contam. Hydrol.*, *71*, 47–66.

S. E. A. T. M. van der Zee, Department of Environmental Sciences, Wageningen University, P.O. Box 8005, 6700 EC Wageningen, Netherlands.

M. I. J. van Dijke, Institute of Petroleum Engineering, Heriot-Watt University, Riccarton Campus, Edinburgh EH14 4AS, UK.

E. L. Wipfler, Netherlands Institute of Applied Geoscience, TNO-NITG, P.O. Box 80015, 3508 TA Utrecht, Netherlands. (l.wipfler@nitg.tno.nl)